

Trade-off between lithium diffusivity and transference in solid ternary polymer ionic liquid electrolytes

Weijers, Mark; Karanth, Pranav; Homann, Gerrit; Izelaar, Boaz; Kondakova, Aleksandra; Ganapathy, Swapna; Kortlever, Ruud; Battaglia, Corsin; Mulder, Fokko M.

DOI

[10.1016/j.ssi.2025.116854](https://doi.org/10.1016/j.ssi.2025.116854)

Publication date

2025

Document Version

Final published version

Published in

Solid State Ionics

Citation (APA)

Weijers, M., Karanth, P., Homann, G., Izelaar, B., Kondakova, A., Ganapathy, S., Kortlever, R., Battaglia, C., & Mulder, F. M. (2025). Trade-off between lithium diffusivity and transference in solid ternary polymer ionic liquid electrolytes. *Solid State Ionics*, 424, Article 116854. <https://doi.org/10.1016/j.ssi.2025.116854>

Important note

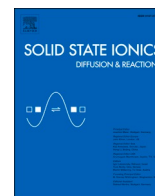
To cite this publication, please use the final published version (if applicable).
Please check the document version above.

Copyright

Other than for strictly personal use, it is not permitted to download, forward or distribute the text or part of it, without the consent of the author(s) and/or copyright holder(s), unless the work is under an open content license such as Creative Commons.

Takedown policy

Please contact us and provide details if you believe this document breaches copyrights.
We will remove access to the work immediately and investigate your claim.



Trade-off between lithium diffusivity and transference in solid ternary polymer ionic liquid electrolytes

Mark Weijers^a, Pranav Karanth^a, Gerrit Homann^{d,e,f}, Boaz Izelaar^c, Aleksandra Kondakova^a, Swapna Ganapathy^b, Ruud Kortlever^c, Corsin Battaglia^{d,e,f}, Fokko M. Mulder^{a,*}

^a Faculty of Applied Sciences, Chemical Engineering Department, Delft University of Technology, Van der Maasweg 9, Delft 2629HZ, the Netherlands

^b Faculty of Applied Sciences, Department of Radiation Science and Technology, Delft University of Technology, Mekelweg 15, Delft 2629JB, the Netherlands

^c Faculty of Mechanical Engineering, Department of Process and Energy, Delft University of Technology, Leeghwaterstraat 39, Delft 2628CB, the Netherlands

^d Empa – Swiss Federal Laboratories for Materials Science and Technology, Überlandstrasse 129, Dübendorf 8600, Switzerland

^e ETH Zurich, Department of Information Technology and Electrical Engineering, Gloriastrasse 35, 8092 Zürich, Switzerland

^f EPFL, School of Engineering, Institute of Materials, Station 7, 1015 Lausanne, Switzerland

ARTICLE INFO

Keywords:

Polymerized ionic liquid
Electrolyte
Transference number
Lithium conductivity
Diffusion
Relaxometry
NMR

ABSTRACT

For battery architectures that need a solid ion conductor with good contacting performance and high stability against electrochemical oxidation, polymerized ionic liquids (PIL) pose a valuable class of materials. The low conductivity of the binary PIL/ lithium salt system can be increased using a ternary ionic liquid acting as plasticiser. The conductive mechanism of the ternary system is however not fully understood. This work shows the shift in conduction mechanism for the ternary Li-/[1,3]PYR-/PDADMA-FSI system by increasing the lithium salt concentration and comparing the transfer mechanism to binary ionic liquid (IL) electrolyte analogues using pulsed field gradient (PFG) nuclear magnetic resonance (NMR), NMR relaxometry, Raman spectroscopy and electrochemical techniques. Two conducting regimes were found which show a strong trade-off between conductivity and transference number. In the low lithium salt regime (≤ 35 wt% LiFSI), cluster diffusion of aggregated lithium is the dominating mechanism leading to low transference numbers (0.04–0.15 at room temperature (RT)). The high salt regime (≥ 50 wt% LiFSI) shows diffusion through free lithium ion hopping transfer, which has a stronger dependence on temperature and yields higher transference numbers (0.31 at RT). Increasing lithium salt concentration shows an inverse linear correlation with conductivity. The electrochemical characteristics of ternary IL/PIL/lithium salt are shown to be highly tuneable by varying the lithium salt fraction, while it maintains excellent characteristics like processability, stability and mechanical function.

1. Introduction

In the search for flexible ionic conducting materials, polymerized ionic liquids (PIL) are a class of solid state electrolytes which have garnered considerable attention in terms of innovation and potential use in lithium ion batteries [1–3]. The advantage of PIL is that one of the ions is incorporated into the polymer chain, resulting in a solid material with conducting properties. To function as a lithium conductor the addition of a lithium salt is needed for cationic PIL, a class of PIL in which the cation is immobilized. Binary PIL/lithium salt show relatively low ionic conductivity ($< \text{mS/cm}$) with a high lithium transference number. For the poly(diallyldimethyl)ammonium fluorosulfonylimide (PDADMAFSI)/lithium fluorosulfonylimide (LiFSI) system, a

conductivity of 0.078 mS/cm with a t_{Li^+} of 0.56 was reported at 80 °C [4]. A secondary ionic liquid (IL) can be added as plasticiser, making it a ternary (PIL:IL:lithium salt, called IL-PIL throughout this work) system. As such, IL-PIL typically offer good ionic conductivity and a high stability against oxidation, good surface contact with electrodes at mild pressures and excellent cycling performance, as shown by Fu et al. [5] They used N-propyl-N-methylpyrrolidinium bis(trifluoromethylsulfonyl) imide ([1,3]PYRFSI) as IL, which cycled for 600 and 300 cycles in lithium metal NMC811 and LNMO full cells, respectively. Pyrrolidinium based PILs therefore form an excellent candidate as the ion-conducting constituent of battery separators and coatings. Recently, Homann et al. showed increased lithium salt concentrations allow improved electrochemical performance in lithium metal NMC811

* Corresponding author.

E-mail address: F.M.Mulder@tudelft.nl (F.M. Mulder).

<https://doi.org/10.1016/j.ssi.2025.116854>

Received 20 December 2024; Received in revised form 20 March 2025; Accepted 30 March 2025

Available online 6 April 2025

0167-2738/© 2025 The Authors. Published by Elsevier B.V. This is an open access article under the CC BY license (<http://creativecommons.org/licenses/by/4.0/>).

full cells [6]. In this work we investigate the mechanism behind the increased lithium conduction of the IL-PIL used in these works by probing molecular motions in a wide range of time scales and lithium salt concentrations.

The system investigated possesses three positively charged ions. The system contains lithium and [1,3]PYR cations and PDADMA cationic polymer. As counterion only one negatively charged ion, being FSI is used. Studies have been conducted on similar systems, optimizing for example Li(T)FSI/[x,y]PYR(T)FSI ILE systems in which x and y depict the alkyl chain length [7,8], or including various polymers focussing on changes in molecular interactions using a fixed ratio of lithium salt to ionic polymer [9]. On a similar, PDADMA(T)FSI based IL-PIL, spin relaxation is studied to investigate local interactions [10]. Here they conclude cationic polymers mechanically stabilize liquid electrolytes with a lower net decrease in lithium motion compared to neutral polymers [10]. Also, comparison between FSI and TFSI combinatory effects [11], the effect of polymer concentration in the IL-PIL TFSI system [12] and the effect of stack pressure [13] have been studied before. Finally, the effect of the [x,y]PYR concentration [14] and the effect of the ratio between IL and PIL have also been studied to find the balance between an increase in diffusivity and the lower transference [15]. One general observation is that increasing the lithium salt in ionic liquids has shown to have a beneficial effect on the transference number and therefore net charge transfer in lithium ion conducting systems [16]. This observation has been exploited to some degree by making high salt PDADMAFSI IL-PIL using phosphonium ionic liquid instead of [1,3]PYRFSI [17]. In this study the concentration of lithium salt is varied to assess the change in effective lithium conduction to find a similar optimum and to understand the underlying mechanism of change in transference number observed between binary and ternary PIL and IL-PIL respectively.

An ideal ionic conductor would only transfer the redox active ion (giving a transference number of 1). Such a material would not suffer from problems arising from concentration depletion, which typically lead to unwanted side reactions at interfaces. Of the solid-state electrolytes, polymers show transference numbers lower than unity due to correlated ionic motion and polymer segmental motion [18]. Adding ionic liquids reduces the transference number further, albeit with the benefit of increased conductivity. By adding a plasticising agent several additional factors can be influencing the PILs transfer numbers and conductivity:

- The lithium ions in IL, PIL, and IL-PIL are surrounded by negative counterions in a solvation shell, affecting its diffusivity [19]. Such a solvation shell may act as clusters which migrate in an electric field to one of the poles depending on the polarity of the cluster [20].
- Ions either present as ionic liquid constituents or part of the polymer chain may affect the formation/dissolution rate of the solvation shell by formation of stable aggregates [21].
- The counter-ion may disturb the inertia of the conducting ion by momentum conservation, which leads to a strong anticorrelated motion and very low transference numbers reported in systems with high lithium salt concentrations [3].
- Segmental motion of the polymer affects ionic migration as well [22].

The mobile cations are able to migrate in the electric field, leading to concentration polarization effects [23]. The role of the polymer in lithium transfer mechanisms has no clear theoretical basis in ternary systems. Analysing the mobilities at different time scales with NMR, compared to electrochemical measurements and Raman spectroscopy (Fig. 1) can elucidate whether the root cause of sluggish transfer lies in the movement of lithium ions as individuals, which potentially allow a transference number of 1 (when the anions are immobilized), or if there is coupled migration.

Local kinetic effects like making/breaking of aggregates, defined by the degree of association, is estimated using NMR relaxometry. The

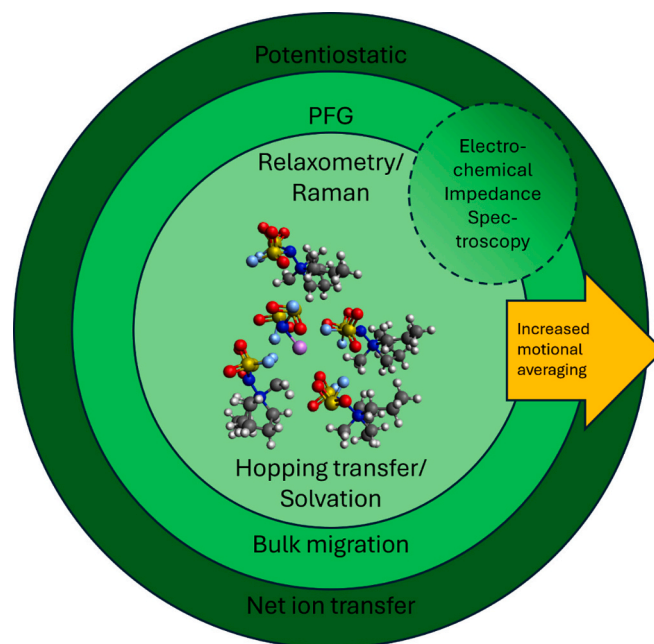


Fig. 1. Description of the correlation between the measurement techniques and the information on molecular motion the technique is able to acquire. The longest time scales shows the net ion transfer originating from the various different types of diffusion phenomena in an electric field. The shortest time scale show the relative molecular motions. In between the intermediate time scale shows the tracer diffusion of specific molecular species. Together the three time scales show which diffusion mechanism is dominating: cluster diffusion dominated (relatively high diffusion coefficient with respect to molecular hopping frequency and a high degree of concentration polarization) or ion hopping dominated (relatively low diffusion coefficient with respect to molecular hopping frequency and a low degree of concentration polarization).

aggregate cluster size is observed by Raman spectroscopy. Long range diffusion effects of aggregates, causing concentration polarization is analysed by comparing electrochemical diffusion coefficients with diffusivities measured through PFG NMR. Finally, this paper correlates the observations to a quantitative theoretical framework proposed by Wohde et. Al. [24] to increase the understanding of ion mobilities in ternary IL-PIL.

2. Experimental

2.1. Electrolyte synthesis

IL-PIL electrolyte separators were made using the procedure of Homann et al. [6]: a 25 μm thick porous polypropylene separator (Celgard 2500) was punched into a disc with a diameter of 18 mm, dried in vacuum ($< 10^{-3}$ mbar) for 12 h, and soaked in a solution containing 1 M LiFSI in [1,3]PYRFSI (60 wt%) and PDADMAFSI (40 wt%) in acetonitrile (ACN, Solvionic, 1:1 wt ratio) for 1 h, dried passively in a polytetrafluoroethylene (PTFE) dish and subsequently soaked again [6]. This procedure was repeated for the other samples after adding LiFSI (99.99 %, Solvionic) to the solution, to increase the salt concentrations summarized in Table 1. In a previous study Yoon et al. found an optimum lithium salt concentration for lithium charge transfer around 3 M LiFSI in [1,3]PYRFSI for the ILE system without polymer [16]. The optimum concentration for maximum lithium conductivity in IL-PIL can be similar to the previously found optimum of the ILE analogue [6]. Therefore, for the IL-PIL system a concentration of 20 wt%, LiFSI (called 20 IL-PIL) was selected, which contain a similar LiFSI/IL ratio to 3 M LiFSI in [1,3]PYRFSI. Similarly, an optimized lithium IL:PIL ratio was used, previously found to be 51:40 wt%, with 9 wt% lithium salt [5,6].

Table 1
Materials used in this study.

Abbreviation based on roundoff % LiFSI	m/m% Polymer PDADMA FSI	m/m% Ionic Liquid [1,3]PYR FSI	m/m% Salt Li FSI	Molarity LiFSI in PIL
10	40 %	51 %	9 %	0.56
20	35 %	44 %	21 %	1.27
35	29 %	37 %	34 %	1.88
50	22 %	28 %	50 %	2.56

Concentrations of 9 wt%, 34 wt% and 50 wt% LiFSI (called 10, 35 and 50 IL-PIL respectively) were tested to determine trends as function of lithium salt concentration.

The infiltrated Celgard separator is then dried at 20 °C in vacuum ($<10^{-3}$ mbar) for 24 h, and transferred into an argon-filled glovebox (see Fig. 1b). Separators (Celgard 3501) were dipped in 1 M and 3 M LiFSI in [1,3]PYR FSI solutions. Separators were fit in between two 12 mm lithium discs in a C2032 coin cell.

2.2. Electrochemical measurements

Electrochemical (EC) measurements were conducted using a PAR-STAT MC200 module (Ametek) and a climate chamber. The cells were conditioned at setpoint temperature in a climate chamber (Memmert) for at least two hours and measured in duplo. Materials were tested in symmetric Lithium coin cell configuration. Electrochemical impedance spectroscopy (EIS) measurements were conducted in a range between 0.1 Hz and 100 kHz with 10 mV amplitude. After a resting period a potentiostatic measurement at 10 mV is conducted for at least 0.5 h (dt = 1 s, 10 ms during first 10 s). The steady state current of the potentiostatic measurement is taken as low frequency point (<0.5 mHz) to obtain steady state resistance R_{SS} calculated from steady state current I_{SS} . The potential relaxation after this period is measured during an hour (dt = 1 s, 10 ms during first 10 s). A second EIS measurement is conducted to check if the cell resistances changed during the period (see example Figure S2).

2.3. Pulse field gradient NMR

For Pulsed field gradient NMR, a Bruker Ascend 600 ($B_0 = 14.1$ T) magnet equipped with a NEO console was used. A 5 mm NMR sample tube was filled with precursor solution described above. Drying was conducted at room temperature in an argon filled glovebox until the majority of acetonitrile was evaporated. To prevent flash boil-up, samples were subjected to stepwise vacuum of 200 mbar intervals with regular intervals of 30 min until full vacuum was reached. After 24 h of drying samples were measured using stimulated echo pulse field gradient procedure on ^7Li for Li^* tracer diffusivity ($\pi/2$ pulse length of 16.8 μs , 45 W and $B_1 = 10\text{--}500$ G/cm for 2 ms), ^{19}F for FSI* tracer diffusivity ($\pi/2$ pulse length of 23 μs , 15.5 $B_1 = 10\text{--}250$ G/cm for 2 ms) and ^1H for [1,3]PYR* tracer diffusivity ($\pi/2$ pulse length of 18 μs , 20.3 W, $B_1 = 64\text{--}1280$ G/cm for 2 ms) using a linear gradient of 8 slices with typical diffusion times of 10–50 μs . Data was fit using the Stejskal-tanner equation [25].

2.4. NMR relaxometry

For NMR relaxometry a Bruker Ascend 500 ($B_0 = 11.7$ T) magnet equipped with a NEO console was used. The sample was filled in an airtight 4 mm rotor zirconia rotor with a vespel cap and inserted in a 4 mm triple resonance MAS NMR probe (Bruker). For ^7Li (194.37 MHz), $\pi/2$ pulse lengths of 3.5–4.5 μs (143.88 W) corresponding to RF field strengths of 71.8–55.5 kHz were utilized. T_1 saturation recovery measurements were performed under static conditions in the temperature range of -40 to 85 °C. Low temperature measurements were conducted

by cooling the variable temperature gas flow through liquid nitrogen as coolant and subsequent heating to the appropriate temperature. Relaxation measurement fitting was performed using the Dynamics Center module from Bruker. Temperature dependent relaxation rate fitting was conducted using the OriginPro 2019 software after deconvolution of the spectra.

In order to estimate the rate of lithium complexation and transfer, spin-lattice (T_1) relaxation measurements can be used to determine the hopping rate and energetics of lithium transfer from one position to another. Similarly, fluorine relaxation can be correlated to the transfer of FSI ions with respect to its surroundings. The change in relaxation rate correlates to the effectiveness at which the nucleus is able to lose its excited state and return to equilibrium. In our case, the Larmor frequency of lithium ($\omega_0 = 194.37$ MHz) and fluorine ($\omega_0 = 470.592$ MHz) in the magnetic field (500 MHz ^1H) which we use, determine the characteristic rate $1/\tau_c$ at a certain temperature T_c , at which the nucleus relaxes fastest in its surroundings. The nuclear relaxation rate at this temperature is most efficient, and generally correlates to the average transfer period of the nucleus from one surrounding to another. When the movement of ions is uncorrelated, this results in a symmetric exponential shape which can be fit using the Bloembergen-Purcell-Pound [26] formulation (Eq. (1)) to obtain the activation energy of the transfer [27]. Here the relaxation period T_1 is fit as function of the hopping time τ and second moment, or interaction strength M_2 .

$$\frac{1}{T_1} = \frac{2}{3}M_2 \left(\frac{\tau}{1 + \omega_0^2\tau^2} + \frac{4\tau}{1 + 4\omega_0^2\tau^2} \right) \quad (1)$$

The hopping period at other temperatures is subsequently estimated using the Arrhenius equation (Eq. (2)), solving τ_0 and E_A . The characteristic hopping period τ_c , having the duration of the inversed larmor frequency, is measured as the fastest relaxation at temperature T_c .

$$\tau = \tau_0 e^{\frac{-E_A}{k_b T}} \quad (2)$$

The relaxometry method yields information on the energetic environment at a specific (relatively high) frequency (short time scale), which combined with PFG can show the correlation of complexation time, diffusivity and transference.

2.5. Raman spectroscopy

Raman spectroscopy was performed on a Horiba Jobin Yvon Lab-RAM HR800 Raman Spectroscopy system, using an excitation wavelength of 515 nm (Cobolt FandangoTM 50) and a 50 \times objective lens. Raman measurements were recorded between 100 and 2000 cm^{-1} and an acquisition time of 20 s and accumulation of 5 using the maximum slit and hole opening (1000) with a grating of 1800. To avoid air exposure, the specimens were transferred (in an Ar glovebox) to an airtight homemade optical sample holder.

2.6. Derivation of transference and conductivity

The transference number during anion blocking condition ($t_{Li^+}^{abc}$, Eq. (3)) is a useful measure to quantify net effective current for lithium ion battery applications in concentrated solutions [28]. The anion blocking transference definition from Vargas-Barbosa and Roling [28] is used which is the ratio of lithium conductivity σ_{Li^+} to total conductivity σ_{tot} which is defined as the sum of lithium and other, residual conductivity σ_{res} . The anion blocking transference compensates for initial current contribution and solid electrolyte interface (SEI) layer resistances, R_{SEI} which varies between interface layer composition, salt concentrations and temperatures. The ratio of lithium conductance in the bulk to the total conductance is calculated using resistances R_{ele} and R_{SEI} obtained from high frequency and inflection point in the EIS spectrum respectively. Steady state resistance R_{SS} is obtained from current j_{SS} under potential U from PITT (Figure S1). Electrolyte resistance R_{ele} is measured

using the high frequency impedance resistance in the EIS spectra. The SEI resistance R_{SEI} is taken as the real resistance readout at the tipping point of the first semicircle (10–50 Hz) in the EIS spectra, minus the electrolyte resistance. Steady state current j_{ss} is taken as the current readout after 12 h of polarization at potential U .

$$t_{Li^+}^{abc} = \frac{\sigma_{Li^+}}{\sigma_{Li^+} + \sigma_{res}} = \frac{\sigma_{Li^+}}{\sigma_{tot}} = \frac{1}{1 + \left(\frac{U}{j_{ss}} - R_{SEI} \right) / R_{ele}} \quad (3)$$

This transference number is compared with the transference determined from diffusivities obtained by PFG (Eq. (4)) [28]. Here the charge is not indicated, as in PFG this cannot be discerned.

$$t_{Li^+}^{PFG} = \frac{\sigma_{Li^+}^*}{\sigma_{Li^+}^* + \sigma_{FSI}^* + \sigma_{13PYR}^*} \quad (4)$$

The tracer conductance (σ^*) of molecule x is calculated using the Nernst Einstein equation.

$$\sigma_x^* = \frac{c_x F^2}{RT} D_x^{PFG}$$

The tracer conductance may be split in an associated ($1 - \alpha$) and dissociated fraction α following Vargas-Barbosa and Roling [28], yielding the lithium ion conductance σ_{Li^+} :

$$\sigma_{Li^+}^* = \alpha \sigma_{Li^+} + (1 - \alpha) \sigma_{LiFSI}$$

In analogy to [28] this can be done with FSI^- and counter ions $13PYR^+$ and $PDADMA^+$ using dissociated fractions β and γ respectively. Since $PDADMA$ is immobile, σ_{PDADMA^+} remains practically zero. The PFG transference becomes Eq. (5).

$$t_{Li^+}^{PFG} = \frac{\alpha \sigma_{Li^+} + (1 - \alpha) \sigma_{LiFSI}}{\alpha \sigma_{Li^+} + \beta \sigma_{13PYR^+} + (\alpha + \beta + \gamma) \sigma_{FSI^-} + 2(1 - \alpha) \sigma_{LiFSI} + (1 - \beta) \sigma_{13PYRFSI}} \quad (5)$$

$$= \frac{\sigma_{Li^+} + s}{\sigma_{Li^+} + \left(1 + \frac{(\beta + \gamma)}{\alpha} \right) \sigma_{FSI^-} + \frac{\sigma_{13PYR}}{\alpha} + 2s}$$

With the variable s indicating the associated fraction to $LiFSI$ as $s = \frac{1 - \alpha}{\alpha} \sigma_{LiFSI}$.

Two ionic transfer mechanisms contribute to the lithium transference number in anion-blocking conditions. The first being through free lithium (cation) migration and the second through neutral pair diffusion with anion migration [28]. Similarly the anion blocking transference is defined as Eq. (6). [28]

$$t_{Li^+}^{abc} = \frac{\sigma_{Li^+} + \frac{s \sigma_{FSI^-}}{(\sigma_{FSI^-} + s)}}{\sigma_{Li^+} + \left(1 + \frac{(\beta + \gamma)}{\alpha} \right) \sigma_{FSI^-} + \frac{\sigma_{13PYR}}{\alpha}} \quad (6)$$

Free lithium cation migration requires the lithium ion to hop from site to site in order to balance the ion transfer happening at the electrode interfaces. For neutral pair diffusion with anion migration there is a dependence on FSI ions hopping to do the same.

Comparison of $t_{Li^+}^{abc}$ and $t_{Li^+}^{PFG}$ in Eq. (5) and Eq. (6) highlights two differences between the techniques. First, the conductivity in $t_{Li^+}^{abc}$ originating from anion migration is not appropriately accounted for in the PFG transference estimation. This mode of conductivity is determined by the degree of association with lithium(s) and motion of free anions σ_{FSI^-} . Second, the degree of association lowering the PFG transference, giving $t_{Li^+}^{PFG} = 0.5$ at high degrees of association $s > \sigma_{ion}$ diverges from the physical behavior of electrolytes in anion blocking conditions. In this work the two values are reported as function of salt concentration to observe which type of migration dominates the mode of transference.

A comparison of tracer diffusivity and effective diffusivity is conducted using PFG and the potential relaxation rate after PITT. For electrochemical diffusivity from potential relaxation generally two ap-

proaches are used [29]. Long term relaxation yields diffusivity estimations near concentration equilibrium. Short term relaxation yield diffusivity estimations which may need concentration correction. Short term relaxation is suitable here due to the relatively short depolarization period over separator thickness L (30 μm) and limited concentration polarization with PITT (5–9 mV dU, where ~ 46 mV/mol was measured in a concentration cell). In the estimation of short relaxation diffusivity $D_{+,eff}$ the slope m of a linear fit of potential readout U versus squared time (Eq. (7)) from $t = 0.5$ to 8 s is used in Eq. (8) [29].

$$U = mt^{1/2} + U_0 \quad (7)$$

$$D_{Li^+,eff} = \frac{\pi L^2}{16} \left(\frac{m}{U_0} \right)^2 \quad (8)$$

The slow potential relaxation ($6 s > t > 10 s$) which does not include activity coefficients does not show linearity upon plotting $\log(U(t))$ and are two orders below the expected diffusivities (Figure S5). The low values obtained using long potential relaxation may origin from the almost complete relaxation of short range polarization, either due to the short pathway (low resolution) or by larger secondary effects like SEI equilibration in the symmetric lithium metal cell after 12 h of potentiostatic measurement.

3. Results

3.1. Transference and conductivity

After acetonitrile evaporation, a transparent Celgard sheet was obtained which was infiltrated with a non-sticky gel for concentrations lower than 50 IL-PIL. The conductivity and transference of the systems are measured in symmetric $Li:Li$ cells through EIS and potentiostatic measurements at various temperatures as is shown in Fig. 2. Similar to the ILE analogue the lithium conduction is the highest in the 20 IL-PIL system (Fig. 2). The $t_{Li^+}^{abc}$ increases with increasing salt concentration to a more typical lithium-salt-in-polymer value of $t_{Li^+}^{abc} = 0.26$. However, for the 35 IL-PIL and 50 IL-PIL material the total conductivity drops severely. Strikingly the transference number of the 10 IL-PIL and 20 IL-PIL systems are not that different compared to the 1 M and 3 M ILE systems (Figure S3). Based on these observations, the role of the polymer seems to have a minimal effect on the transference number at these concentrations.

Increasing the temperature does typically increase the total conductivity and may cause divergence of the transference number when the mobilities of the constituents have a different temperature dependence. The total conductivity σ_{tot} of 20 IL-PIL is in the same order compared to 10 IL-PIL as function of temperature (Fig. 2B). With increasing salt concentrations, the σ_{tot} becomes generally lower. The observed optimum of $\sigma_{Li,RT}$ for 20 wt% $LiFSI$ concentration in 20 IL-PIL remains. However σ_{Li^+} shows a different temperature dependence between the different salt concentrations. At 333 K, the 50 IL-PIL σ_{Li} even exceeds the 35 IL-PIL σ_{Li} due to its high transference number.

Elevated temperatures generally show a positive effect on the transference number (Fig. 2A, EC lines). This positive influence is stronger for higher salt concentrations. The activation energy for lithium transfer generally appears to be higher compared to the other conducting constituents, which translates to an increasing transference as function of temperature for all materials tested. The plasticising effect of 1,3PYRFSI increases the mobility of all constituents, yielding a higher conductivity σ_{res} for lower $LiFSI$ fraction IL-PILs. Immobilization of the FSI anion, which may yield transference numbers above 0.5 are not observed.

A comparison of the transferences measured electrochemically and derived from PFG NMR provides insight into the mode of transport and utilization of ion mobility in the material (Fig. 2A, PFG lines). Only for 35 IL-PIL the $t_{Li^+}^{PFG}$ shows a negative trend as a function of temperature. In

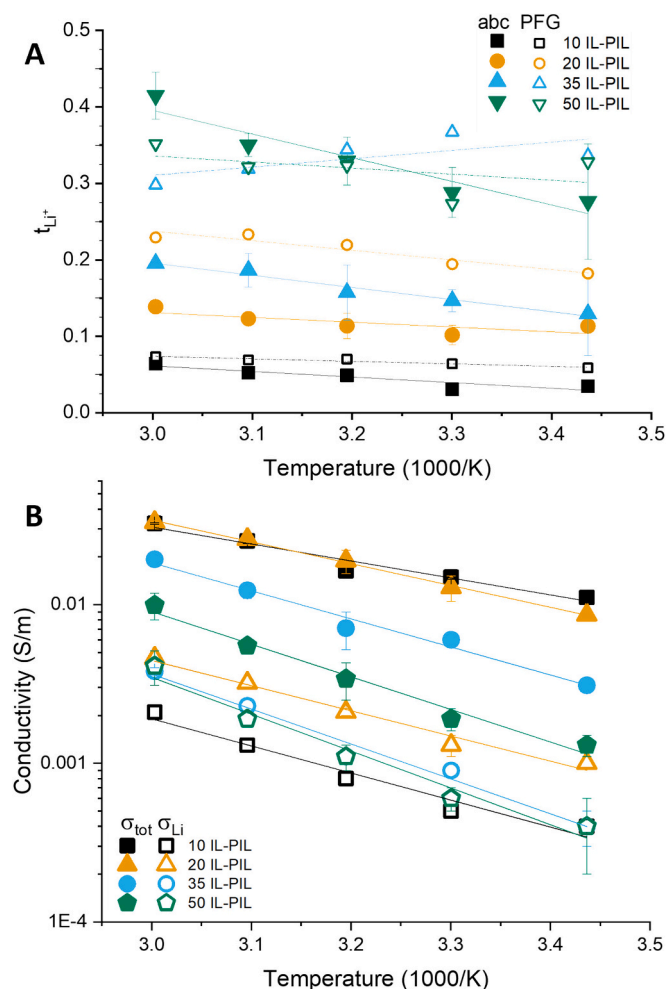


Fig. 2. (A) Transference number obtained electrochemical under anion blocking condition $t_{Li^+}^{abc}$ compared to transference number $t_{Li^+}^{PFG}$ obtained from PFG NMR and (B) total ionic conductivity σ_{tot} and lithium-ion conductivity σ_{Li} of IL-PILs with varying LiFSI concentration as a function of temperature. With higher lithium salt concentration the contribution of lithium conductivity increases. Error bars indicate difference between duplic measurement.

this system the FSI* tracer conductance is increasing more at higher temperatures compared to the other tracer conductivities in this material. The anion blocking transference $t_{Li^+}^{abc}$ is generally found to be lower compared to $t_{Li^+}^{PFG}$ (Fig. 2A) for all materials tested and both values are below 0.5. This behavior is expected to originate from a high mobility of ion pairs compared to dissociated ions (SI Figure S4). A $t_{PFG} < 0.5$ is expected only with a relatively high mobility of secondary cations, like [1,3]PYR⁺. An exception to the comparatively lower $t_{Li^+}^{abc}$ is the 50 IL-PIL, which shows a $t_{Li^+}^{abc}$ which is equal or higher than $t_{Li^+}^{PFG}$. Based on Eq. (5) and Eq. (6), an increasing $t_{Li^+}^{PFG}$ can be explained by a lower conductivity of [1,3]PYR* or if the transfer mechanism of free lithium starts to dominate. The tracer diffusivities of Li* and FSI* as a function of temperature remain the same order of magnitude for all LiFSI concentrations tested (Fig. 3A). Also the ratio of [1,3]PYR*/Li* diffusivity remains similar (0.76 for 10 IL-PIL and 0.56 for 50 IL-PIL, Figure S11), indicating a small decrease in the specific [1,3]PYR* diffusivity. The total conductivity σ_{tot} does however drop, indicating less mobility of conducting ions while the specific lithium conductivity σ_{Li} does not show much difference (Fig. 2B). Therefore in this case, conduction through free lithium ions appears to become a significant part of the charge transfer mechanism in anion blocking condition.

Differences between tracer diffusivity D_{PFG} and effective diffusivity

D_{EC} obtained through electrochemical potential relaxation show the degree of correlated motions of ions by e.g. association/solvation or repulsion. For IL-PIL the tracer diffusivity of Li* and FSI* has a strong dependence on temperature and are in the same order of magnitude in the complete temperature range (Fig. 3A). However, D_{EC} (Fig. 3B) is an order of magnitude lower and shows only a weak dependence on temperature. A temperature dependence similar to D_{PFG} with increasing salt concentrations is not observed in the potential relaxation method. This indicates that D_{PFG} does not adequately represent the ion motion during depolarization of the electrolyte. PFG measurements do not probe association as it directly traces the bulk migration of the NMR sensitive nucleus in the applied magnetic field gradient only. Therefore the observed difference between tracer and effective diffusivities may originate from a high degree of association of lithium to the FSI counterion.

The temperature dependence of D_{PFG} (Fig. 3A/B, ⁷Li for Li* and ¹⁹F for FSI*) and conductivities σ_{Li} and σ_{tot} (Fig. 2) were fitted using the Arrhenius equation yielding the activation energy $E_{A,diff}$ and $E_{A,EC}$ respectively (Fig. 3C). Activation energies of the total conductivity $E_{A,EC,tot}$ and FSI* tracer diffusivity $E_{A,diff,FSI}$ show a similar temperature dependence for both processes. The activation energies show a trend that is in line with viscous behavior. Upon the addition of polymers or kosmotropic (order-making, interaction enhancing) salts in poly-electrolyte solutions, an increase in the viscosity is observed due to higher constrained mobility and lowered electrostatic repulsion [30]. Such constraints cause an increased dependence on temperature, which is observed in the IL-PIL series as well. The change in activation energy of FSI* tracer diffusivities $E_{A,diff,FSI}$ are smaller compared to the change in $E_{A,EC,tot}$ but show a similar trend. Upon addition of the polymer the FSI diffusion activation energy $E_{A,diff,FSI}$ shows a significant decrease, which is not translated to a decrease of $E_{A,EC,tot}$ (Fig. 3C, ¹⁹F of 1 M ILE versus 10 IL-PIL). This indicates that the FSI⁻ anion becomes less dependent on changes of ordering when the polymer is introduced.

The temperature dependence of lithium diffusion and conduction point to multiple modes of lithium transfer. Similar to lithium diffusion $D_{diff,Li}$ the temperature dependence of lithium conduction σ_{Li} decreases when the polymer is introduced ($E_{A,diff,Li}$ and $E_{A,EC,Li}$ Fig. 3C between 1 M ILE versus 10 IL-PIL). However, the temperature dependence of lithium conductivity $E_{A,EC,Li}$ seems to follow the trend of $E_{A,EC,tot}$ above 10 IL-PIL concentration rather than $E_{A,diff,Li}$, which hints the conduction mechanism at these concentrations is not solely dependent on lithium ion diffusion. For ILE this trend in activation energy is similar: a higher LiFSI concentration results in a lower temperature dependence of lithium diffusivity while it shows an increased temperature dependence for lithium conductivity (following the total conductivity). In Fig. 3C the activation energies for lithium conductivity $E_{A,EC,Li}$ of 20 IL-PIL shows a lower temperature dependence compared to both lower and higher salt concentrations 10 IL-PIL and 35 IL-PIL respectively. A second observation is that the lower temperature dependence of lithium diffusion $E_{A,diff,Li}$ in 50 IL-PIL compared to 35 IL-PIL does not translate to a lower temperature dependence of lithium conductivity $E_{A,EC,Li}$. This highlights PFG NMR measurements are not sufficient to predict the mode of conduction in ternary systems as lithium association plays a strong role in the conduction mechanism.

3.2. Solvation and Raman

Raman spectroscopy is used to study the solvation environment of lithium ions in the IL-PIL system when the LiFSI concentrations are increased. The S-N-S symmetric stretching vibration of FSI is often used to obtain information about the Li⁺ – FSI⁻ coordination modes. These modes are typically categorised as solvent-separated ion pairs (SSIP at 720 cm⁻¹), contact ion pairs (CIP at 730 cm⁻¹) and aggregates (AGG I at 739 cm⁻¹ and AGG II at 752 cm⁻¹) [31–33]. According to the literature, diluted LiFSI based electrolytes (< 0.25 LiFSI/solvent ratio) result in predominantly SSIP and CIP Raman bands, while the peaks associated

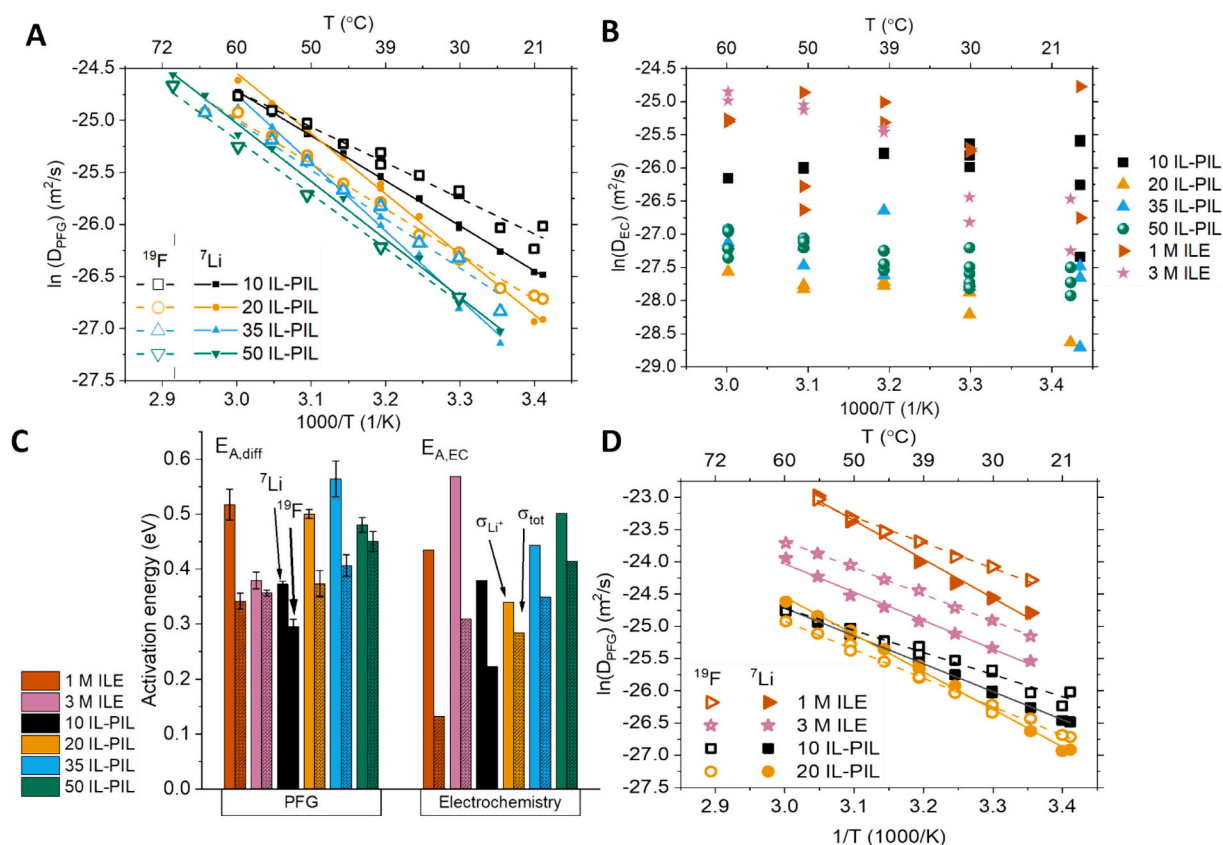


Fig. 3. Temperature dependence of Lithium and FSI Diffusivities of IL-PILs and ILE from 20 to 60 °C. A) Lithium (${}^7\text{Li}$) and FSI (${}^{19}\text{F}$) tracer diffusivity in PILs obtained through PFG NMR. B) Effective electrochemical diffusivity $D_{\text{Li}^+, \text{eff}}$ obtained by fast potential relaxation measurements. C) Activation energies obtained by fitting Arrhenius equation on tracer diffusivities (left), lithium and total conductivities (right). D) Lithium (${}^7\text{Li}$) and FSI (${}^{19}\text{F}$) tracer diffusivity of PILs compared to their ILE analogue.

with $\text{Li}^+ - \text{FSI}^-$ aggregates become more present at moderate-to-higher salt concentrations [31]. A similar trend is observed in our Raman spectra in Fig. 4. The lowest LiFSI concentration at 10 IL-PIL shows a signal at lower Raman shifts, matching well with SSIP and CIP coordination modes. Peak broadening was observed at 20 IL-PIL, indicating the coexistence of different types of ionic – solvent interactions, which did not change when the LiFSI concentration is increased to 35 IL-PIL. This result is not surprising since the transference number barely changed (Fig. 2A) between 20 and 35 IL-PIL. At 50 IL-PIL, the $\text{Li}^+ - \text{FSI}^-$ environments are mostly in their aggregated states. The 50 IL-PIL shows phase transitions at -16.3 (2.03 J/g) and -0.9 °C (1.77 J/g) with DSC (Figure S7, using a heating rate of 10 °C/min), where lower concentrations only show a change in specific heat below -15 °C, but show no clear phase transition between -35 and 100 °C. The phase transition of 50 IL-PIL, together with the low aggregation indicates LiFSI is near its glass transition state.

3.3. Spin lattice relaxation

The duration of lithium association to its counterion is probed by measuring the differences in relaxation rate in NMR relaxometry for the Li and the counterion. This yields the Li^+ and FSI^- hopping frequency which is the inverse of the complexation time (Fig. 5A and B respectively). The peak maxima (drop down lines) indicate the temperature at which the hopping frequency is equal to the Larmor frequency of the nucleus probed. The fluorine spectrum (Fig. 5B) highlights that this characteristic frequency occurs at higher temperatures with increasing salt concentration. This indicates a lowered mobility within the solvation complex when the LiFSI salt concentration is increased. The ILE indicate increased hopping frequency compared to the IL-PIL analogues

(Fig. 5B, dashed drop down lines).

The characteristic lithium hopping rate does not follow the same trend compared to fluorine, when increasing the salt concentration: above 20 wt% LiFSI with increasing LiFSI mass fraction the characteristic rate does not change significantly (Fig. 5A, drop down lines). The relaxation rate increases (Fig. 5A, peak height), but that illustrates an increasing dipolar interaction strength, not the timescale of the mobility itself. As the FSI^- hopping frequency decreases as a function of salt concentration, this results in a net increase in the lithium hopping rate. This may explain the higher transference numbers at increasing lithium salt concentrations. Lithium mobility in ionic liquids show generally a higher characteristic rate compared to the IL-PIL analogues (Fig. 5A). The BPP model for NMR spin-lattice relaxation shows a good fit with a single uncorrelated hopping transfer process (Fig. 5, fitting lines). The peak symmetry indicates that lithium transfers occurs via a single transfer process between equal (or indistinguishable) states of aggregation during nanosecond intervals. The model fit results in the activation energy for transfer $E_{A, \text{trans}}$ (Fig. 5C) which allow extrapolation of the characteristic hopping rate at temperatures other than T_C using the Arrhenius equation.

To test if the mode of conduction is through neutral pair displacement, the anion blocking transference can be correlated to the displacement of lithium in a complex. The duration of a complex can be estimated by taking the inverse of the lithium hopping frequency, which yields characteristic duration of a complex τ . When τ is multiplied by the tracer diffusivity of lithium $D_{\text{Li}}^{\text{PFG}}$ this yields the neutral displacement τD_{Li} (Fig. 5D).

To increase the mechanistic understanding, Wohde et. Al [24] proposed a quantitative method to distinguish correlated movement of lithium originating from counterions (by associative movements) and

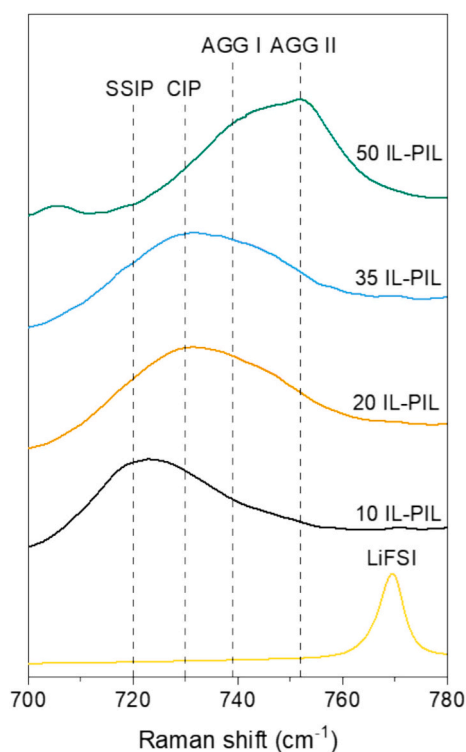


Fig. 4. Raman spectra of the S-N-S stretching vibration between 700 and 780 cm^{-1} for various LiFSI concentrations (given in wt%) in IL-PIL at room temperature. Different $\text{Li}^+ - \text{FSI}^-$ ion pairing modes, such as solvent-separated ion pairs (SSIP, 720 cm^{-1}), contact ion pairs (CIP, 730 cm^{-1}) and aggregates (AGG I at 739 cm^{-1} and AGG II at 752 cm^{-1}) are identifiable with an increase in the LiFSI concentration and match well with ref. 32–33.

cation-cation and/or anion-anion interactions. This approach relates the anion blocking transference to the complex duration using parameter ξ as the degree of correlated movement via Eq. (9) [24]. Here ϕ is defined as the degree of non-ideality originating from cation-cation correlations, and $(1 - \phi)$ as the degree of non-ideality from anion-anion correlations. Here the case of equal contributions of cation-cation and anion-anion non-idealities is tested which result in $\phi = t_{\text{Li}^+}^{\text{PFG}}$.

$$t_{\text{Li}^+}^{\text{abc}} = \frac{\xi^2 - 4\phi + 4\phi^2}{4(1 - \phi)(1 - \xi)} \quad (9)$$

As expected a negative correlation appears between lithium complex displacement τ^*D_{Li} and transference (Fig. 5D). Two outliers are observed. The 50 IL-PIL (Fig. 5D, indicated with Δ) indicates lithium complex displacement is not dictating the mode of transference $t_{\text{Li}^+}^{\text{abc}}$ as it does not follow the trend of lithium complex displacement found for other IL-PIL concentrations (Fig. 5D, line). A change in mode of conductance by free lithium ions when LiFSI becomes the major mass fraction of the material is expected. This could result in strong cation-cation (anti)correlations in which case Eq. (9) would not be applicable. In concordance, the solvation of lithium (Fig. 4) and hopping transfer energy $E_{\text{A,trans}}$ (Fig. 5C) increases significantly for the 50 IL-PIL compared to lower LiFSI weight fractions. This indicates a higher energy is needed for breaking up the more strongly bound aggregates observed with Raman (Fig. 4). In contrast, the change in $E_{\text{A,trans}}$ for PILs does not change significantly for concentrations below 50 %wt LiFSI.

The second outlier is at 10 IL-PIL (Fig. 5C, circle with asterisk) which shows a poor correlation between complexation, transference and the degree of association. It must be noted that during relaxometry acquisition of 10 IL-PIL, samples which were held above approximately 70 °C repeatedly showed an increasing instead of a decreasing Li relaxation rate during ramping down of the temperature (Figure S7). The

relaxation time becomes similar to ionic liquids with a maximum relaxation rate at a lower temperature. This may indicate that a (local) phase separation occurred, which is not visible in differential scanning calorimetry (DSC) measurements (Figure S8). Phase separation of 10 IL-PIL at high temperatures may have influenced determination of the τ_c , implying longer complexation times, as T_C was never reached during heating. When a similar characteristic temperature T_C as 20, 35 and 50 IL-PIL are assumed the correct correlation between τ^*D_{Li} and $t_{\text{Li}^+}^{\text{abc}}$ becomes apparent (Fig. 5D, open triangle/square).

4. Conclusion

The conduction mechanism of salts dissolved in polymers can be understood by correlating the polymer's rheologic behavior and carrier concentration to the conductive performance of the solvated ions [34]. Ternary polymer ionic liquids show different behavior as the ionic liquid cation lowers the effective transference but increases the mobility of all constituents to a great extent. In this work a range of lithium salt concentrations are tested to understand the role of the ionic liquid cation in constructive and anticorrelated motion of the lithium ion.

The energetics of the ionic lithium complex formation, as observed by relaxometry, remain unchanged with increasing lithium salt concentration until the lithium salt becomes the dominant fraction in 50 PIL. Below this concentration a contribution from the presence of the polymer in the gel is not apparent in the lithium transfer process, as the activation energy of transfer is not altered. Tracer diffusivity of FSI, being the counterion of all cation constituents, forms a good indicator for the change in mobility by viscosity changes in the polymer gel. The activation energy of conduction shows a strong correlation to the FSI diffusivity. The conduction mechanism can therefore be described as 'cluster diffusion dominated'. Positive correlations of transference to the degree of association ξ imply a significant contribution of neutral carriers' mobility. A dramatic shift in both relaxation behavior and solvation of lithium is observed in 50 IL-PIL, indicating a strong shift in lithium transfer mechanism. The transfer may be described as 'hopping transfer dominated' originating from free lithium ion conduction at these concentrations, as AGG II aggregation state dominates for this concentration.

The high temperature dependence of mobility in 'dilute' lithium-ion concentrations in ionic liquids as observed in PFG NMR becomes smaller when the polymer is introduced. Increasing the lithium salt concentration in the ternary systems reverses this effect. The activation energy of lithium diffusivity in the 20 IL-PIL shows a local minimum between this trade-off, and electrochemical measurements show a local optimum of lithium conductivity at room temperature for this material. The increased net lithium conductivity of 20 IL-PIL indicates an optimal balance between the carrier concentration, correlated motion and viscosity below 60 °C. Generally the diffusivity of lithium in IL-PILs are lower compared to the ILE, which may be explained by the severe change in material viscosity.

IL-PILs can be deposited on (electrode) substrates using wet processing techniques and therefore pose a valuable material for use as lithium conductor in solid state batteries. This work shows that depending on the desired transference number and conductivity one can select the lithium salt concentration to have the desired conduction mechanism. At high temperatures the lithium conductivity consistently increases with higher weight fractions of the conducting salt. At lower temperatures there exists an optimum which balances the mobility and lithium concentration. For high temperature lithium battery applications (40–60 °C) IL-PIL with high conducting salt concentrations have the benefit of showing high transference numbers as well.

CRediT authorship contribution statement

Mark Weijers: Writing – original draft, Visualization, Methodology,

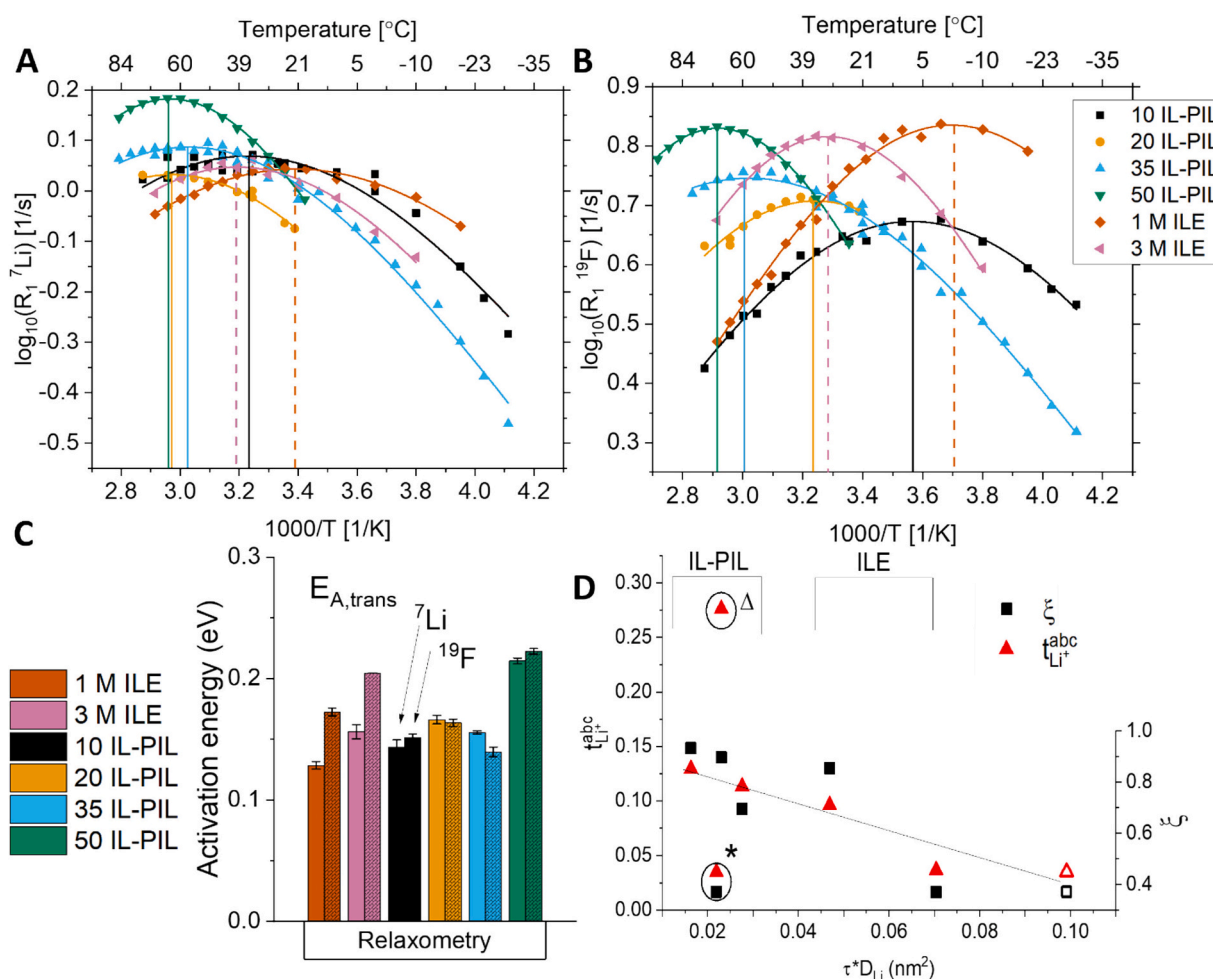


Fig. 5. ${}^7\text{Li}$ (A) and ${}^{19}\text{F}$ (B) NMR Relaxometry on IL-PIL and ILE. The change in relaxation rate R_1 as function of temperature indicate the change in spin-lattice motion of the nucleus at its larmor frequency. Line indicates the fit of the BPP model. Activation energies obtained by the BPP model fit (C) and correlation between transference and RMS displacement estimation using PFG diffusivity and characteristic hopping time at 30 °C (D). Line is added in (D) to guide the eye. Open triangle/square indicates implied RMS displacement of 10 IL-PIL (encircled with asterisk), when similar τ_c as 20 IL-PIL is assumed as phase changes occurred at temperatures above 70 °C during relaxometry. 50 IL-PIL is second outlier indicated with Δ symbol.

Investigation, Formal analysis, Data curation, Conceptualization. **Pra-nav Karanth:** Writing – review & editing, Methodology, Investigation. **Gerrit Homann:** Conceptualization. **Boaz Izelaar:** Writing – review & editing, Investigation. **Aleksandra Kondakova:** Investigation. **Swapna Ganapathy:** Writing – review & editing, Supervision, Resources. **Ruud Kortlever:** Resources. **Corsin Battaglia:** Writing – review & editing, Conceptualization. **Fokko M. Mulder:** Writing – review & editing, Resources, Project administration, Funding acquisition.

Declaration of competing interest

The authors declare that they have no known competing financial interests or personal relationships that could have appeared to influence the work reported in this paper.

This project has received funding from the European Union's Horizon 2020 research and innovation programme under grant agreement No. 875557. Neither the European Commission nor any person acting on behalf of the Commission is responsible for how the following information is used. The views expressed in this publication are the sole responsibility of the authors and do not necessarily reflect the views of the European Commission.

Acknowledgements

This project has received funding from the European Union's Horizon 2020 Research and Innovation Programme under grant agreement No. 875557. Neither the European Commission nor any person acting on behalf of the Commission is responsible for how the following information is used. The views expressed in this publication are the sole responsibility of the authors and do not necessarily reflect the views of the European Commission.

Molecular visualization in graphical abstract is made using Avogadro: an open-source molecular builder and visualization tool. Version 1.2.0. <http://avogadro.cc/> [35]

Appendix A. Supplementary data

Supplementary graphs for this article can be found here. Data for this article, including raw Raman, Electrochemical, DSC, and formatted NMR are available at 4TU at <https://doi.org/10.4121/0bd878cd-0d1d-420e-b424-aad2782cb616>.

Data availability

Data for this article, including raw Raman, Electrochemical, DSC, and formatted NMR are available at 4TU at [doi](https://doi.org/10.4121/0bd878cd-0d1d-420e-b424-aad2782cb616).

org/10.4121/Obd878cd-0d1d-420e-b424-aad2782cb616

References

- [1] A.S. Shaplov, R. Marcilla, D. Mecerreyes, *Electrochim. Acta* 175 (2015) 18–34.
- [2] G.G. Eshetu, D. Mecerreyes, M. Forsyth, H. Zhang, M. Armand, *Mol. Syst. Des. Eng.* 4 (2019) 294–309.
- [3] J.C. Barbosa, D.M. Correia, R. Gonçalves, V. de Zea Bermudez, S. Lanceros-Mendez, C.M. Costa, *Mater. Chem. Front.* 7 (2023) 5046–5062.
- [4] F. Makhlooghiyazad, L. Miguel Guerrero Mejía, G. Rollo-Walker, D. Kourati, M. Galceran, F. Chen, M. Deschamps, P. Howlett, L.A. O'Dell, M. Forsyth, *J. Am. Chem. Soc.* 146 (2024) 1992–2004.
- [5] C. Fu, G. Homann, R. Grissa, D. Rentsch, W. Zhao, T. Gouveia, A. Falgayrat, R. Lin, S. Fantini, C. Battaglia, *Adv. Energy Mater.* 12 (2022) 2200412.
- [6] G. Homann, Q. Wang, S. Liu, A. Devincenti, P. Karanth, M. Weijers, F.M. Mulder, M. Piesins, T. Gouveia, A. Ladam, S. Fantini, C. Battaglia, *A.C.S. Appl. Energy Mater.* 7 (2024) 10037–10043.
- [7] I. Nicotera, C. Oliviero, W.A. Henderson, G.B. Appetecchi, S. Passerini, *J. Phys. Chem. B* 109 (2005) 22814–22819.
- [8] M. Moreno, E. Simonetti, G.B. Appetecchi, M. Carewska, M. Montanino, G.-T. Kim, N. Loeffler, S. Passerini, *J. Electrochem. Soc.* 164 (2017) A6026–A6031.
- [9] M. Brinkkötter, E.I. Lozinskaya, D.O. Ponkratov, P.S. Vlasov, M.P. Rosenwinkel, I. A. Malyschkina, Y. Vygodskii, A.S. Shaplov, M. Schönhoff, *Electrochim. Acta* 237 (2017) 237–247.
- [10] M. Brinkkötter, M. Gouverneur, P.J. Sebastião, F. Vaca Chávez, M. Schönhoff, *Phys. Chem. Chem. Phys.* 19 (2017) 7390–7398.
- [11] M. Martínez-Ibañez, N. Boaretto, L. Meabe, X. Wang, H. Zhu, A. Santiago, O. Zugazua, M. Forsyth, M. Armand, H. Zhang, *Chem. Mater.* 34 (2022) 7493–7502.
- [12] M. Gouverneur, S. Jeremias, M. Schönhoff, *Electrochim. Acta* 175 (2015) 35–41.
- [13] A. Agrawal, S. Yari, H. Hamed, T. Gouveia, R. Lin, M. Safari, *Carbon Energy* 5 (2023) e355.
- [14] A.-L. Pont, R. Marcilla, I. De Meazza, H. Grande, D. Mecerreyes, *J. Power Sources* 188 (2009) 558–563.
- [15] G.B. Appetecchi, G.-T. Kim, M. Montanino, M. Carewska, R. Marcilla, D. Mecerreyes, I. De Meazza, *J. Power Sources* 195 (2010) 3668–3675.
- [16] H. Yoon, P.C. Howlett, A.S. Best, M. Forsyth, D.R. MacFarlane, *J. Electrochem. Soc.* 160 (2013) A1629–A1637.
- [17] X. Wang, H. Zhu, G.M.A. Girard, R. Yunis, D.R. MacFarlane, D. Mecerreyes, A. J. Bhattacharyya, P.C. Howlett, M. Forsyth, *J. Mater. Chem. A* 5 (2017) 23844–23852.
- [18] M.P. Rosenwinkel, M. Schönhoff, *J. Electrochem. Soc.* 166 (2019) A1977–A1983.
- [19] P. Martínez-Crespo, M. Otero-Lema, O. Cabeza, H. Montes-Campos, L.M. Varela, *J. Mol. Liq.* 359 (2022) 119188.
- [20] D.M. Pesko, K. Timachova, R. Bhattacharya, M.C. Smith, I. Villaluenga, J. Newman, N.P. Balsara, *J. Electrochem. Soc.* 164 (2017) E3569–E3575.
- [21] S. Chen, S. Zhang, X. Liu, J. Wang, J. Wang, K. Dong, J. Sun, B. Xu, *Phys. Chem. Chem. Phys.* 16 (2014) 5893–5906.
- [22] K.M. Diederichsen, E.J. McShane, B.D. McCloskey, *ACS Energy Lett.* 2 (2017) 2563–2575.
- [23] T. Gao, J. Itliong, S.P. Kumar, Z. Hjorth, I. Nakamura, *J. Polym. Sci.* 59 (2021) 2434–2457.
- [24] F. Wohde, M. Balabajew, B. Roling, *J. Electrochem. Soc.* 163 (2016) A714–A721.
- [25] E.O. Stejskal, J.E. Tanner, *J. Chem. Phys.* 42 (1965) 288–292.
- [26] N. Bloembergen, E.M. Purcell, R.V. Pound, *Phys. Rev.* 73 (1948) 679–712.
- [27] A.F. McDowell, N.L. Adolphi, C.A. Sholl, *J. Phys. Condens. Matter* 13 (2001) 9799–9812.
- [28] N.M. Vargas-Barbosa, B. Roling, *ChemElectroChem* 7 (2020) 367–385.
- [29] J. Landesfeind, J. Hattendorff, A. Ehrl, W.A. Wall, H.A. Gasteiger, *Spectroscopy. J. Electrochem. Soc.* 163 (2016) A1373–A1387.
- [30] N.B. Wyatt, C.M. Gunther, M.W. Liberatore, *Polymer* 52 (2011) 2437–2444.
- [31] S.-D. Han, O. Borodin, D.M. Seo, Z.-B. Zhou, W.A. Henderson, *J. Electrochem. Soc.* 161 (2014) A2042–A2053.
- [32] H. Iriawan, A. Herzog, S. Yu, N. Ceribelli, Y. Shao-Horn, *ACS Energy Lett.* 9 (2024) 4883–4891.
- [33] T.D. Pham, A. Bin Faheem, K. Lee, *Small* 17 (2021) 2103375.
- [34] S.S. Sekhon, *Bull. Mater. Sci.* 26 (2003) 321–328.
- [35] M.D. Hanwell, D.E. Curtis, D.C. Lonie, T. Vandermeersch, E. Zurek, G.R. Hutchison, *J. Chemother.* 4 (2012) 17.